THE JOURNAL OF PHYSICAL CHEMISTRY C
A JOURNAL OF THE AMERICAN CHEMICAL SOCIETY

pubs.acs.org/JPCC

Article

Disentangling Light- and Temperature-Induced Thermal Effects in Colloidal Au Nanoparticles

Lijie Wang, Davood Zare, Tsz Him Chow, Jianfang Wang, Michele Magnozzi, and Majed Chergui*

Cite This: *J. Phys. Chem. C* 2022, 126, 3591−3599

Read Online

ACCESS | Metrics & More | Article Recommendations | Supporting Information

ABSTRACT: We present temperature-dependent (from room temperature to 80 °C) absorption spectra of Au/SiO_2 core−shell nanoparticles (NPs) (core diameter: ∼25 nm) in water in the range from 1.5 to 4.5 eV, which spans the localized surface plasmon resonance (LSPR) and the interband transitions. A decrease in absorption with temperature over the entire spectral range is observed, which is more prominent at the LSPR. These changes are well reproduced by theoretical calculations of the absorption spectra, based on the experimentally measured temperature-dependent real (ε_1) and imaginary (ε_2) parts of the dielectric constant of Au NPs and of the surrounding medium. In addition, we model the photoinduced response of the NPs over the entire spectral range. The experimental and theoretical results of the thermal heating and the simulations of the photoinduced heating are compared with the ultrafast photoinduced transient absorption (TA) spectra upon excitation of the LSPR. These show that while the latter is a reliable monitor of heating of the NP and its environment, the interband region mildly responds to heating but predominantly to the population evolution of charge carriers.

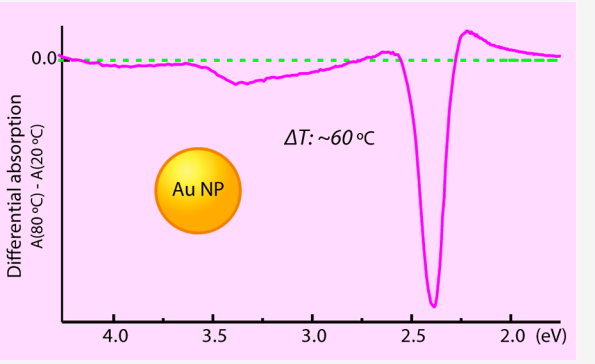

INTRODUCTION

Noble metal nanoparticles (NPs) have intensely been studied since the 1990s due to their potential and actual applications in areas such as photovoltaics (in the case of NP-sensitized transition-metal oxides),[1−3] photocatalysis,[4−6] medical imaging,[7−9] cancer therapy,[10,11] and so forth. The key aspect of these applications is the exploitation of the intense localized surface plasmon resonance (LSPR) absorption band in the visible range and the physical phenomena ensuing its excitation by light. Because noble metal NPs can be engineered in different shapes and sizes, there is a degree of flexibility in tuning the LSPR band energy and width, in order to suit a given application. Furthermore, the fact that the environment also affects the LSPR adds an extra degree of freedom to the tuning.

The above applications are fundamentally governed by the generation of charge carriers and heat upon the photoexcitation of the LSPR band. Indeed, photoexcitation generates charge carriers above the Fermi level of the metal, which after electron−electron (few tens to hundreds of femtoseconds) and electron−phonon scattering (few picoseconds) transfer their energy to the lattice. The latter then dissipates it to the environment at longer times.[5] Depending on the type of application, either charge carrier generation or heat generation are favored. In particular, in the case of the heat generation under optical irradiation, numerous promising applications are envisioned or already implemented in energy conversion,[12,13] catalysis,[5,14] and medicine.[10,11] One of the exciting aspects of these studies is that the NP can be a nanolocal source of heat.

The heating of noble metal NPs under either continuous or pulsed irradiation of the LSPR has been investigated by several authors.[12,15−21] In these studies, the LSPR band itself is used to monitor the temperature of the NPs, either dissolved in a colloidal solution or embedded in a matrix (glass, sol−gel, mesoporous film, or other).[22−33] Ultrafast spectroscopy has been (and still is) the most frequently used tool to investigate the details of the electron and thermal evolutions in metallic materials, either in the bulk, or NP form.[5,21,24,34−43] In these studies, monitoring the LSPR response was achieved by transient absorption (TA) in the case of NPs or transient reflectivity (TR) in the case of bulk materials, using a broadband continuum probe. The measured transient signal is the difference ΔA (ΔR) of the absorption (reflectivity) after excitation with the signal before. Usually, a depletion of the LSPR band around its center (i.e., a negative signal) and the appearance of positive features in the wings characterize the response, pointing to a broadening

Received: December 22, 2021
Revised: January 31, 2022
Published: February 14, 2022

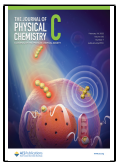

https://doi.org/10.1021/acs.jpcc.1c10747
J. Phys. Chem. C 2022, 126, 3591−3599

of the LSPR band.[21,35,36] Most of the signal recovers on a 2−3 ps time scale, leaving a weak component decaying in tens to hundreds of picoseconds. More recently, O'Keeffe et al.[43] used an approach combining the post-processing of the fs TA measurements guided by the so-called semiclassical extended two-temperature model, allowing the isolation of the purely non-thermal contribution to the pump−probe experimental map recorded for 2D arrays of Au nanoellipsoids. They thus demonstrated the intimate correlation between electron energy and probe photon energy on the ultrafast time-scale of electron thermalization. However, their study was limited to the region of the LSPR.

While the LSPR band is dominated by the Drude part of the dielectric function, at energies higher than the LSPR, the absorption spectrum of Au NPs is due to the so-called interband region (Figure S1), which originates from band-to-band transitions. In a recent paper, we presented for the first time ultrafast TA studies of typically 20 nm diameter aqueous Au NPs, monitoring the response of the interband transitions.[39] This response consisted of positive and negative TA bands that were characterized by a temporal evolution comparable to that of the LSPR. The TA features were interpreted using the band structure (BS) diagram of bulk Au, considering that the quantum size effects in Au occur for particle sizes below ∼4 nm.[44,45] It was concluded that the response reflects a slow cooling of the charge carriers, which is concurrent with the thermal cooling of the lattice, that is on the order of 150−250 ps. Our analysis assumed the linear response, that is, the interband transitions are affected by the transient electron and hole occupation numbers. However, in a study of the TR of Au films probed in the region of the LSPR, Kruglyak et al.[46] rationalized the response of the system by calculations that account for the full dependence of the reflectivity on the electron occupation number. They concluded that the bipolar behavior of the reflectivity signals does not necessarily contain a contribution from non-thermalized electrons, as had previously been assumed.[47] However, the latter is not self-consistent because TR and transmission signals appear to have a different temporal shape[48] and hence cannot be both proportional to the same function of time, for example, the transient electron temperature. Further to this, Stoll et al.[49] investigated the response of the environment to the cooling of LSPR-excited Au NPs and showed that depending on the probe wavelength, different kinetics arise due to the involvement of the environment, which they successfully modeled using the thermal conductance at the metal−liquid interface and the heat diffusion in the liquid.

The studies by Kruglyak et al.[46] and Stoll et al.[49] raise questions as to whether the photoinduced TA changes in the region of interband transitions may also be due to the temperature-induced changes of their dielectric function and/or a response of the environment.

The complex interplay between the electronic and thermal effects in the LSPR response of photoexcited Au NPs, can best be tackled by performing temperature-dependent steady-state absorption spectra of the NPs, comparing them to photoexcited spectra. This was recently done by Ferrera et al.[21] who carried out an ultrafast study of the optical response of 2D arrays of Au NP (20−25 nm) films in the region of the LSPR and compared them to temperature-dependent studies. The temperatures ranged from room temperature (RT) to 660 K. By comparing the differential temperature-dependent spectra (difference of the steady-state spectrum at a given temperature minus that at RT) with the TA spectra at different pump fluences, they could extract a thermometric calibration scale of ultrafast processes in the NPs. This was further supported by an independent model of the temperature-dependent differential spectra. The comparison and the modeling assume that the energy deposited in the NPs by light excitation is all converted into heat.

The major difference between the temperature-induced and light-induced effects is that in the latter case, electrons are transferred above the Fermi level and heat is generated by way of electron−electron and electron−phonon scattering, while in the temperature-driven case, the lattice is at a thermal equilibrium with the heated solvent and any changes that occur should reflect the thermally induced modifications of the dielectric function of the NP. Apart from the above study by Ferrera et al.,[21] few groups have investigated the temperature-dependence of the absorption of Au NPs in detail.[21,44,50,51] The overall effect of heating is a decrease of absorption intensity of the LSPR, accompanied by weak red shifts of a few 10 s meV and broadenings spanning ∼100 meV. These observations were rationalized using a theoretical model that accounts for the electron−phonon scattering in the NP, its thermal expansion, and the temperature dependence of the dielectric permittivity of the host material.[50]

The temperatures used in the above-mentioned studies[21,44,50,51] were well above the boiling point of water. However, in view of the various biomedical applications (imaging, cancer therapy, etc.), it is crucial to characterize the NP response in aqueous media. Surprisingly, such studies are almost completely lacking, except for two partial reports.[20,52] Therefore, in this work, we present for the first time a systematic study of the temperature dependence of the absorption spectrum of aqueous colloidal Au NPs between 20 and 80 °C, over the entire spectral range encompassing the LSPR and the interband transitions. Due to the difficulties (in particular, aggregation) in investigating bare colloidal Au NPs in water, we focus on aqueous Au/SiO_2 NPs (Figure S2). The experimental results show that the temperature-induced changes are dominant at the LSPR band while the interband region is less affected. This is confirmed by the very good agreement with the simulated temperature-dependent spectra, which were carried out using recently reported[53] temperature-dependent spectroscopic ellipsometry results of ∼20 nm Au NPs. We also simulated the photoinduced response in the UV−visible absorption spectrum of the NP following ref 49, which further confirm that temperature effects (whether by quasi-static heating or impulsive laser heating) on the dielectric response of the interband transitions are negligible in the photoinduced TA spectra, supporting our previous conclusion of slow charge carrier cooling.[39] The overarching conclusion of this work is that while the LSPR response is a reliable monitor of the various heating mechanisms of photoexcited NPs, the interband transition region is mostly sensitive to charge carriers and shows barely any effects due to heating.

METHODS AND MODELS

Sample Preparation. *Preparation of Bare Au NPs.* The Au NP samples were synthesized through a seed-mediated growth method.[54] Specifically, a cetyltrimethylammonium bromide (CTAB) solution (0.1 M, 9.75 mL) was first

https://doi.org/10.1021/acs.jpcc.1c10747
J. Phys. Chem. C 2022, 126, 3591−3599

mixed with a $HAuCl_4$ solution (0.01 M, 0.25 mL), followed by the rapid injection of a freshly prepared, ice-cold $NaBH_4$ solution (0.01 M, 0.60 mL) under vigorous stirring. The resultant solution was kept under gentle stirring for 3 h at RT. The as-prepared seed solution (0.24 mL) was injected into a growth solution made of the CTAB solution (0.1 M, 19.5 mL), deionized water (380 mL), $HAuCl_4$ (0.01 M, 8 mL), and ascorbic acid (0.1 M, 30 mL) afterward. The reaction mixture was gently mixed well and left undisturbed overnight at RT. The resultant Au NP samples were washed and concentrated three times by centrifugation and re-dispersion into water for further use.

Preparation of the Au/SiO_2 NPs. CTAB molecules adsorbed on Au NPs were first replaced by thiol-terminated methoxy poly(ethylene glycol) (mPEG-SH). The Au NP solution (100 mL) was centrifuged and re-dispersed in water (20 mL). Then, mPEG-SH (molecular weight: 5000, polymer chain concentration 1 mM) solution (2 mL) was subsequently added. The resultant solution was kept undisturbed at 25 °C for 12 h and then centrifuged twice to remove the excess mPEG-SH polymers. The obtained mPEG-coated Au NPs were re-dispersed in a solution mixture containing 4.5 mL of water, 15 mL of absolute ethanol, and 0.3 mL of $NH_3{\cdot}H_2O$ (30 wt %). After that, 0.08 mL of the silica precursor solution (5 vol % tetraethylorthosilicate in absolute ethanol) was injected into the Au NP solution under ice-cold and ultrasonication conditions for 1.5 h. For the temperature-dependent absorption measurements, the Au/SiO_2 NPs were sonicated for 3 h to eliminate agglomeration.

The morphology of the samples was observed by transmission electron microscopy (TEM) on an FEI Tecnai Spirit microscope operated at 120 kV. Figure S2 shows representative TEM images of the Au/SiO_2 NPs, which were synthesized by growing SiO_2 shell on pre-grown Au NPs. They show well-defined core−shell nanostructures with a clear boundary between the Au core and the SiO_2 shell. The diameter of the NPs is ∼65 nm with a ∼25 nm diameter Au core and ∼20 nm thickness SiO_2 shell.

Steady-State Spectroscopy. *Temperature-Dependent Steady-State Spectra.* The steady-state absorption spectra were recorded with a commercial UV−vis spectrometer (Shimadzu, UV-3600). In order to vary the temperature of the sample, we used a temperature controller connected with a heating unit inside the spectrometer chamber. A water flow was used to adjust and stabilize the temperature. A diagram of the top and side views of the heating unit is shown in Figure S3. The cuvette used here is a commercial Starna 10 mm UV-quartz rectangular cell with a small glass-coated magnetic stir bar inside. The absorption spectra were recorded from RT (∼25 °C) to 80 °C in steps of 10 °C, while the NPs in solution were magnetically stirred.

To convert the nm scale of the absorption spectra into an eV scale, we followed the Jacobian conversion method.[55] The wavelength was converted to energy using $E = hc/\lambda$, and the signal values themselves must be scaled by (hc/E^2), where E represents the photon energy, h is the Planck constant, c is the light speed, and λ represents the wavelength.

Modeling the Temperature-Induced Spectral Response of NPs. To rationalize the temperature-dependent steady-state spectra, we simulated them taking into account the temperature dependence of the complex dielectric function of Au NPs.[53] For relatively small NPs (∼25 nm in diameter), such as those used in the present experiments, the absorption coefficient is written as[56,57]

$$A(\omega) = \frac{9p\varepsilon_d(\omega)^{3/2}}{c} \frac{\omega\varepsilon_2(\omega)}{[\varepsilon_1(\omega) + 2\varepsilon_d(\omega)]^2 + \varepsilon_2(\omega)^2} \quad (1)$$

where $\varepsilon_{Au}(\omega) = \varepsilon_1(\omega) + i\varepsilon_2(\omega)$, ω is the energy. p is the particle volume fraction and is very small ($\ll$1) for particles dispersed in a colloidal solution and ε_d is the dielectric constant (a real quantity) of the surrounding medium, which is water and SiO_2 in the present case. The change in the Au NP sample absorption ΔA depends on changes of ε_1, ε_2, and ε_d. We use the recently reported[53] detailed temperature-dependent spectroscopic ellipsometry study of 2D arrays of ∼20 nm Au NP closely packed in parallel rows and supported on a nanopatterned LiF substrate under high vacuum. The temperature was varied from RT to 350 °C and the spectral range spanned from 245 to 1450 nm. The temperature dependence of the experimental real and imaginary parts of ε_{Au} reported are shown in Figure S4a,b. Note the very different scales of the real (ε_1) and imaginary (ε_2) parts of the permittivity. However, the scale of the

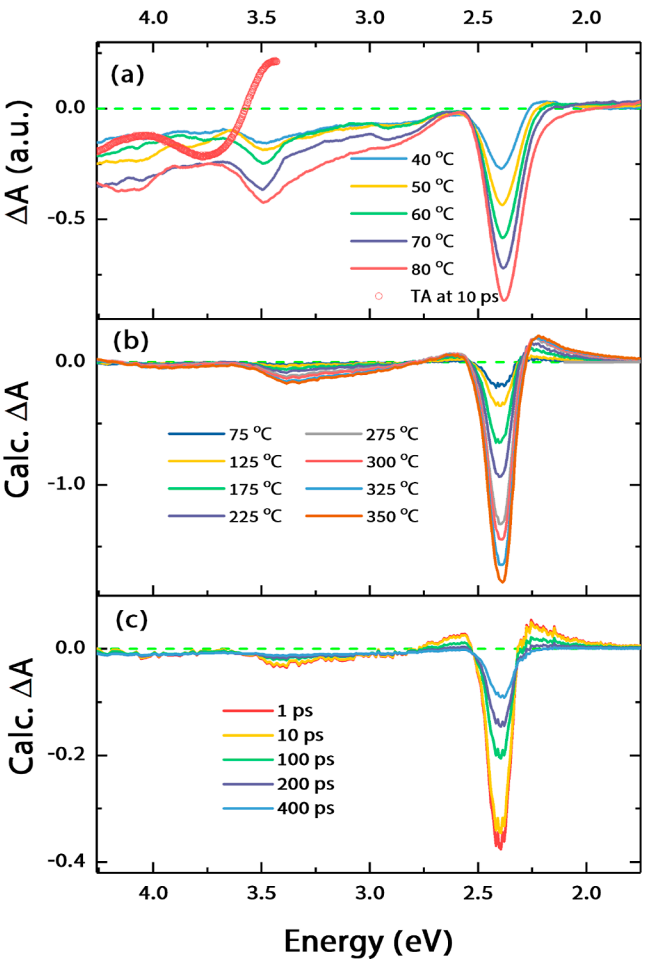

Figure 1. (a) Absorption difference spectra of Au/SiO_2 NPs, obtained by taking the difference of a spectrum at high temperatures minus that at RT (∼25 °C). The red dots represent the UV-probed TA spectrum recorded at 10 ps;[39] (b) calculated differential absorbance of Au NPs from the measured real (ε_1) and imaginary (ε_2) parts of ε_{Au} at temperatures varied from 75 to 350 °C; and (c) calculated TA response upon impulsive heating, reflecting the temperature evolution of the Au NP and the environment.

https://doi.org/10.1021/acs.jpcc.1c10747
J. Phys. Chem. C 2022, 126, 3591−3599

change is similar for both but the trends are opposite in that the (ε_1) decreases, while (ε_2) increases with temperature. Note that in the region of the LSPR (2.2−2.6 eV), the changes of (ε_2) are generally more prominent at the red end than at the blue one, while in the interband transition region, the changes are only significant around 3.5 eV.

The calculation of the absorption spectra based on the above equation neglects the temperature dependence of the ε_d of the surrounding medium as it was shown to play a negligible role in the temperature range 17−915 °C[48] but accounts for its wavelength dependence.[55−61] As surrounding medium, we only consider water because the volume fraction due to the SiO_2 shell is negligible.

Modeling the Photoinduced Spectral Response of NPs. The calculation is based on the model established by Stoll *et al.*[49] A uniform NP temperature T_p is assumed, whose evolution is given by

$$\Delta T_p(t) = 2/\pi k(Rg)^2 \Delta T_0 \times \int_0^{+\infty} \frac{u^2 e^{-hu^2 t/R^2}}{(u^2(1+Rg) - kRg)^2 + (u^3 - kRgu)^2}\, du \tag{2}$$

where ΔT_0 (an initial temperature of 100 °C was used in the simulations) is the initial temperature increase of the NP after the optical pump excitation of the metal electron gas and internal thermalization with the lattice, $h = \Lambda_m/c_m$, $k = 3c_m/c_p$, and $g = G/\Lambda_m$, the related parameters are taken from ref 49.

For the environment, the temperature evolution is given by

$$\Delta T_m(r,t) = \Delta T_0 2R/(r\pi)k(Rg)^2 \int_0^{+\infty} \frac{u e^{-hu^2 t/R^2}\left(u(1-u^2/(kRg))\cos\left(\frac{u(r-R)}{R}\right) + \left(1 - \frac{u^2(1+Rg)}{kRg}\right)\sin\left(\frac{u(r-R)}{R}\right)\right)}{(u^2(1+Rg) - kRg)^2 + (u^3 - kRgu)^2}\, du \tag{3}$$

where r is the environment distance to the NP core, in practice, we used $r = 1.5R$, $2R$, $2.5R$, and $3R$. Because the actual cooling dynamics lead to the nonuniform temperature distribution in the environment, it can be modified into

$$\sum_{i=1}^{N} A_m^i(\lambda_{probe}) \Delta T_m^i(t) \tag{4}$$

with ΔT_m^i being the temperature increase in the i shell in the above equation and A_m^i its associated weight.

The time- and probe wavelength (λ_{probe})-dependent evolution of a NP is related to its ultrafast modifications (via T_p and dielectric function, $\varepsilon_{Au}(\omega) = \varepsilon_1(\omega) + i\varepsilon_2(\omega)$, the dielectric data are taken from ref 62) and those of the environment (via T_m and ε_m)

$$\begin{aligned}\Delta A(\lambda_{probe}, t) &= \left(\frac{\partial \sigma_{ext}}{\partial \sigma_1}(\lambda_{probe})\frac{d\varepsilon_1}{dT_p}(\lambda_{probe}) + \frac{\partial \sigma_{ext}}{\partial \sigma_2}(\lambda_{probe})\frac{d\varepsilon_2}{dT_p}(\lambda_{probe})\right)\Delta T_p(t) \\ &\quad + \left(\frac{\partial \sigma_{ext}}{\partial \sigma_m}(\lambda_{probe})\frac{d\varepsilon_m}{dT_m}\right)\Delta T_m(t) \\ &= A_p(\lambda_{probe})\Delta T_p(t) + A_m(\lambda_{probe})\Delta T_m(t)\end{aligned} \tag{5}$$

RESULTS AND DISCUSSION

We performed a temperature-dependent steady-state absorption study under dark conditions. Figure S1 compares the absorption spectra of bare Au and core−shell Au/SiO_2, normalized at the maximum of the LSPR. They are overall analogous and both exhibit the LSPR band at ∼2.3 eV although the core−shell NPs have a weak (∼0.03 eV) red shift compared to bare Au NPs due to the presence of the SiO_2 shell, while the growing featureless continuous absorption on the high energy side is due to interband transitions and to scattering. The absorption spectra of core−shell Au/SiO_2 NPs measured between RT and 80 °C are shown in Figure S5a. The temperature effect is overall weak and is mostly visible in the region of the LSPR (Figure S5b), where it shows a downward trend in intensity and a slight broadening. The region around 3.5 eV also shows some variations. The temperature effect is best visualized by plotting the differential absorption spectra (spectrum at a higher temperature minus that at RT). These spectra are displayed in Figure 1a. They show a decrease in intensity at the LSPR with increasing T, as well as a decreased intensity over the entire UV region above 2.6 eV. Figure 2a zooms into the region of the LSPR and Figure S6a shows a selection of normalized spectra in the same region. One notes that the intensity drop of the LSPR band increases by a factor of ∼3 between 40 and 80 °C. The minimum of the LSPR signal shifts slightly to lower energies with increasing T and a weak positive wing appears on the red side of the LSPR, with the point where the signal is zero (i.e., $\Delta A = 0$) shifting to lower energies with increasing T. Finally, no positive wing shows up on the blue side of the LSPR band. The trends shown in Figure 1a are qualitatively similar to those reported by Bouillard et al.[51] for Au nanorods. They are also comparable to those reported by Ferrera et al.[21] on 2D arrays of NPs, except that the blue wing in their differential spectra are more prominent than the red one, contrary to our case.

The region of interband transitions in Figure 1a is much less affected by heating than the LSPR region. It exhibits a feature appearing at ∼3.5 eV and the changes in the interband region are monotonous with a decrease of absorption with temperature. The decreasing background signal is likely caused by an increased scattering.

We used eq 1 to simulate the temperature-induced changes of the steady-state spectra, and the result in Figure S7 shows the simulated steady-state absorption spectra, whose variations are exclusively due to the temperature- and wavelength dependence of the dielectric functions. An overall decrease in intensity with increasing temperature is observed over the entire spectral range and is more pronounced at the LSPR maximum (at ∼2.4 eV), while a weaker decrease is visible around ∼3.4 eV. The calculated differential spectra are shown in Figure 1b and a zoom in the region of the LSPR is

https://doi.org/10.1021/acs.jpcc.1c10747
J. Phys. Chem. C 2022, 126, 3591−3599

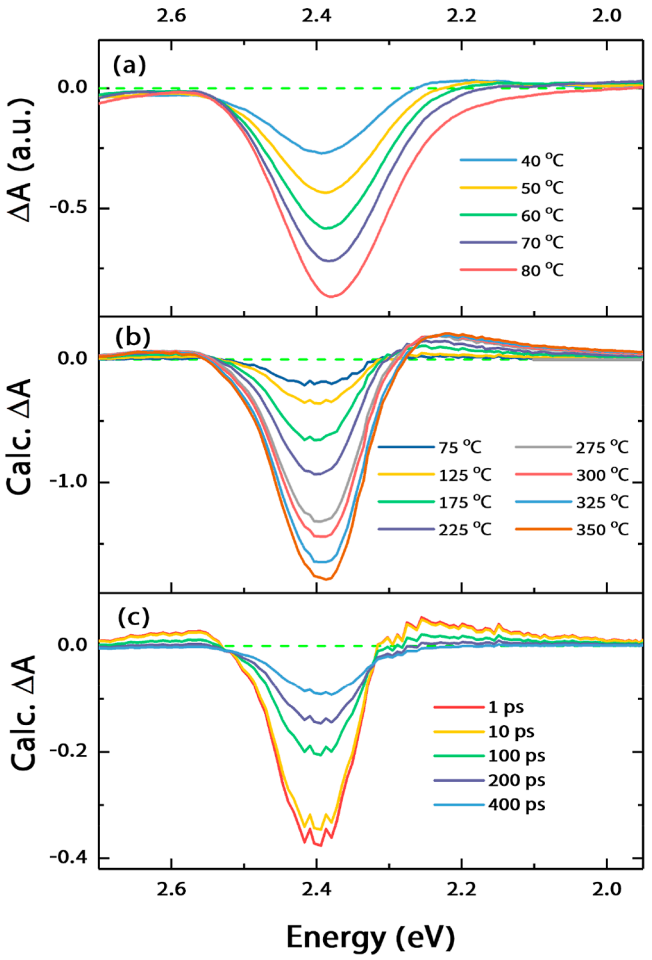

Figure 2. Zoom in the LSPR region of the absorption difference spectra of aqueous Au/SiO_2 NPs: (a) obtained by taking the difference of a spectrum at high temperatures minus that at RT (~25 °C); (b) calculated temperature-induced changes using the measured real (ε_1) and imaginary (ε_2) parts of ε_{Au} at temperatures varied from 75 to 350 °C; and (c) calculated photoinduced changes using the same parameters as ref 49. The noise in the simulated spectra is propagated from the original ellipsometry data shown in Figure S6.

presented in Figure 2b. Because the lowest two temperatures reported by Magnozzi et al. are 25 and 75 °C,[53] the first differential spectrum is at 75 °C, which is close to the highest temperature reached in our experiment in water. Furthermore, it should be stressed that the arrays of NPs, on which the ellipsometry study was carried out,[53] are quite different from the present one because the NPs are closely packed such that a strong electromagnetic coupling is present.[63] Moreover, the substrate was nanopatterned on LiF. For all these reasons, we cannot perform a quantitative comparison between the experimental and calculated differential spectra. However, the main goal here is in reproducing the trends.

Figure S6b shows the normalized calculated differential spectra. From Figures 1, 2 and S6, one notes that the LSPR minimum is somewhat slightly blue-shifted compared to the experimental data, which reflects the shift reported in the steady-state spectra of bare and core−shell Au/SiO_2 NPs (Figure S1). In addition, a positive feature appears on the red side of the LSPR band, as in the experiment (though much more prominent), and its $\Delta A = 0$ point shifts to lower energies with increasing temperature, as our experimental trends show. However, in the temperature-dependent studies of 2D arrays of Au NPs,[21] the opposite was observed. On the blue side, even though the experimental differential spectra do not show a positive wing of the LSPR, the calculations predict one, which is however much weaker than on the red side, in agreement with the changes of ε_2 in this range (Figure S4b). The absence of a blue wing in the experimental data is presumably due to the overall intensity decrease in the range above the LSPR band (Figure 1a). The point at which the differential signal is zero (i.e., $\Delta A = 0$) in the simulated spectra of the blue wing shifts to higher energies with increasing T (Figure S6b).

The temperature-dependent studies of the absorption spectrum of Au NPs embedded in SiO_2[50] and of 2D arrays of NPs[21] are overall consistent with an intensity drop of the LSPR, accompanied by an intensity increase of both its red and blue wings. Unfortunately, in ref 50, the authors did not present differential spectra, which would have been preferable for comparing the trends with our data. Nevertheless, in Figure 3b, we present our simulations of the LSPR

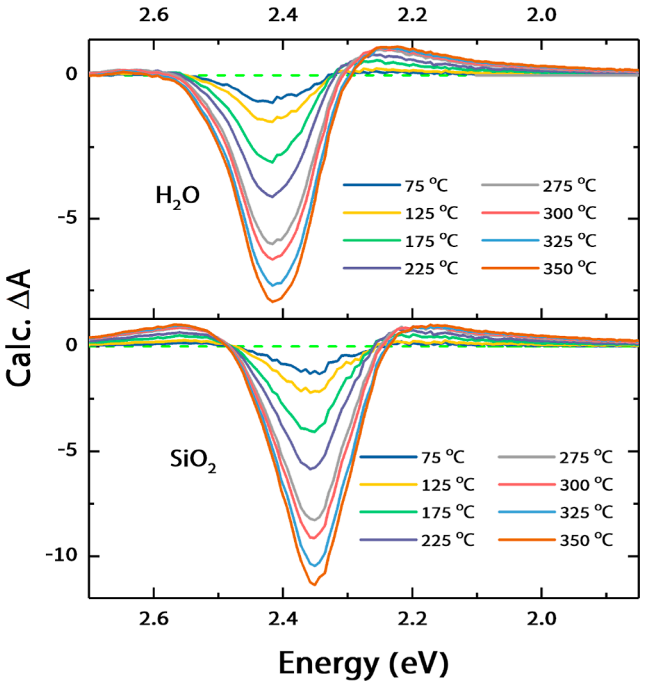

Figure 3. Calculated differential absorbance of Au NPs from the measured real (ε_1) and imaginary (ε_2) parts of ε_{Au}, in different surrounding media: (top) pure water and (bottom) SiO_2. The maximum of the red wings (at 350 °C) are normalized to 1 for comparison.

differential spectra embedded in an SiO_2 glass (the simulated differential spectra over the entire spectral range are shown in Figure S8). Contrary to the case of water but along the trends on 2D arrays,[21] a blue wing clearly shows up (even at the lowest temperature above RT, see Figure S9), with an almost isosbestic $\Delta A = 0$ point and a comparable intensity compared to the red wing. However, for the latter, the $\Delta A = 0$ point moves to higher energies with increasing temperatures in the case of the 2D arrays.[21] The results shown in Figure 3 underscore the fact that the differential spectra are

https://doi.org/10.1021/acs.jpcc.1c10747
J. Phys. Chem. C 2022, 126, 3591−3599

in addition strongly determined by the properties of the medium and not just by those of the NP.

The observations in ref 50 had been rationalized using a model that accounts for the electron-phonon scattering in the NP, its thermal expansion, and the temperature dependence of the dielectric permittivity of the host material. As the temperature increases, so does the NP volume and therefore, the density of free electrons decreases, which in turn leads to a lower LSPR frequency, that is, its red shift. The rate of electron−phonon scattering increases with temperature, which implies an increased damping constant of the plasmon oscillations and as a result a broadening of the LSPR band. Finally, the increase of the dielectric permittivity of silica with temperature also contributes to the red shift of the LSPR, although the main contribution to this shift comes from the volume expansion of the NP.[50] A shift of the LSPR maximum would give rise to a first derivative line shape, while a broadening would give rise to a second derivative line shape, which would be symmetric if the LSPR band is symmetric.

The calculated differential spectra confirm the weak temperature dependence found in the steady-state experiments (Figure 1a), except for the background, which we believe is due to scattering contributions resulting from the SiO_2 shell and the solvent. The simulations also confirm the occurrence of a negative feature around ∼3.35 eV, which would correspond to the negative feature around ∼3.5 eV in the experimental differential spectra (Figure 1a). It is important to stress once more that the calculated spectra span a much higher temperature range than the experiment implying that heat only mildly affects the absorption in the interband region.

Turning now to photoinduced TA, these have been reported for Au NPs in SiO_2 glasses,[24] sol−gel matrix,[23] embedded in mesoporous TiO_2,[32,33] in 2D arrays,[21] and in water[35,39,49,64,65] and ethanol[49] or TR of bulk Au films.[66] All exhibit a profile with a decreased absorption of the LSPR and red and blue wings, often (but not always) with an isosbestic $\Delta A = 0$ on the blue wing and on the red side and a shifting one as a function of time.

In the case of NPs in SiO_2 glasses,[24] the TA spectra were nicely fit using the Mie scattering theory, in order to extract the temporal changes of electron temperatures and effective damping constants. It was concluded that at early times, the nonlinear response originates mainly from the hot electron system generated by the pump pulse but that the lattice temperature also plays an important role even in these first steps of the nonlinear response. Finally, the more recent comparative study of the photoinduced and temperature-induced LSPR absorption changes of Au NPs[21] provided a calibration of the light-induced heating. In the studies of Au NPs in water and ethanol,[49] it was found that the kinetics around the LSPR depended on the probe wavelength, an observation that was rationalized taking into account the heat transfer from the NP to the solvent and the subsequent evolution of the solvent temperature as a function of time and distance from the NP center.

We repeated the calculations of ref 49 using the same parameters that apply to our case but extended the simulations to the deep-UV spectral region. The calculations are described in detail in the Methods and Models section (eqs 2−5). The estimated increase of the lattice temperature is ∼87 °C under our excitation conditions (see Supporting Information, §S1) and in our simulations, we used an initial temperature (upon photoexcitation) of 100 °C. The relevant simulations plots are presented in Figures S11−S13. Figure S12 shows the evolution of the simulated transient transmission as a function of time for different probe energies, decomposed into contributions from the NP, and the environment. It can be seen that the most significant change at 2.4 eV is due to the NPs, with a decay time of ∼250 ps, exactly the value we reported in our previous contribution.[39] At a probe energy of 3.5 eV, the evolution is somewhat slightly slower due to a relatively more prominent contribution from the environment. Figure S13 shows the normalized temperature evolution of the NP and the medium at different radii from the NP center. The simulated spectra are shown in Figures 1c and 2c. They strongly resemble the steady-state temperature-induced differential spectra (Figure 1b), even though we start off from a non-equilibrium situation where the NP is at 100 °C at $t = 0$. In particular, we note that the interband region is little affected, while the LSPR is on the contrary strongly affected. The difference with the photoinduced TA in the interband region[39] is striking. In the TA study,[39] we observed very clear features in the interband region, and the TA spectrum at 10 ps time delay is plotted in Figure 1a. Contrary to the differential temperature-induced spectra and simulated photoinduced heating response (Figure 1b,c) that are generally featureless, the photoinduced TA spectrum exhibits prominent negative features at ∼3.8 and ∼4.4 eV and a positive one at ∼3.5 eV. Following an initial decay on a ∼2−3 ps time scale (just as for the LSPR), these bands exhibit longer decay times on the order of 150−250 ps, along with coherent phonon oscillations. We attributed them to transitions between different points of the Brillouin zone in the BS diagram (see Figure S10), namely, the interband transitions $L_2 \rightarrow L_1$ (∼4.4 eV) and $X_4 \rightarrow X_1$ (∼3.8 eV) and the intraband $L_6 \rightarrow L_3/L_5 \rightarrow L_2$ (∼3.5 eV).

As already mentioned, the major difference between thermodynamic and photoinduced heating is that in the former case, the particles and the surrounding medium temperatures are at equilibrium, while in the TA experiments, only the electrons in the metal are excited, while the surrounding medium is initially cold (Figures S12 and S13). This was shown to affect the transients at probe wavelengths away from the LSPR due to the gradual heating of the medium.[49] Based on Figure 1, one concludes that thermal effects, be they temperature- or photoinduced, have little effect on the interband transitions.

In summary, the good agreement between the experimental and calculated temperature- and photoinduced differential spectra (Figures 1 and 2) supports the conclusion that the photoinduced TA spectra in the interband region cannot be rationalized in terms of thermal effects on the dielectric constants of the NPs or the environment. Therefore, we confirm our previous interpretation of the deep-UV TA changes as reflecting charge carrier relaxation.[39]

CONCLUSIONS

In summary, we presented a temperature-dependent (from RT to 80 °C) investigation of the absorption spectrum of Au/SiO_2 core−shell NPs in the range from the visible (where the LSPR band lies) to the deep-UV (where the interband transitions are found). A decrease in absorption with the temperature over the entire spectral range is observed that is significantly more prominent in the region of the LSPR than

https://doi.org/10.1021/acs.jpcc.1c10747
J. Phys. Chem. C 2022, 126, 3591−3599

that of the interband transitions. These changes are well reproduced by the theoretical calculations of the absorption spectra based on the experimentally measured temperature dependence of the real (ε_1) and imaginary parts (ε_2) of the Au NP dielectric constant and of the surrounding medium. Comparing the temperature-induced experimental and simulated absorption spectra and the simulated photoinduced spectra, as well as those from the literature, and the experimental photoinduced TA spectra suggest that the response of the LSPR band is sensitive to temperature effects on the dielectric function of the NPs reflecting heating of the nanoparticle lattice and of the medium. However, in the interband region, the strong deviation of the differential spectra with the TA one suggests that the latter are dominated by the response of the charge carriers, confirming the interpretation given in ref 39, that is, the reflect a slow charge carrier relaxation.

■ ASSOCIATED CONTENT

Supporting Information

The Supporting Information is available free of charge at https://pubs.acs.org/doi/10.1021/acs.jpcc.1c10747.

Estimation of the initial NP temperature in TA experiments, simulated transient heating response of the NP and environment, temperature-dependent steady-state absorption results, TEM images of the core−shell samples, normalized experimental and calculated differential absorption difference spectra, experimental temperature-dependent real (a) and imaginary (b) parts of ε_{Au} of Au NPs, simulated absorption spectra at different temperatures, BS diagram of bulk Au, computed temperature evolutions at 3.5 eV and at 2.4 eV, computed temperature evolutions in the particle, and at different locations in the environment (PDF)

■ AUTHOR INFORMATION

Corresponding Author

Majed Chergui − *Laboratory of Ultrafast Spectroscopy, ISIC and Lausanne Centre for Ultrafast Science (LACUS), École Polytechnique Fédérale de Lausanne (EPFL), CH-1015 Lausanne, Switzerland;* orcid.org/0000-0002-4856-226X; Email: majed.chergui@epfl.ch

Authors

Lijie Wang − *Laboratory of Ultrafast Spectroscopy, ISIC and Lausanne Centre for Ultrafast Science (LACUS), École Polytechnique Fédérale de Lausanne (EPFL), CH-1015 Lausanne, Switzerland*

Davood Zare − *Laboratory of Ultrafast Spectroscopy, ISIC and Lausanne Centre for Ultrafast Science (LACUS), École Polytechnique Fédérale de Lausanne (EPFL), CH-1015 Lausanne, Switzerland;* Present Address: Faculty of Science—Chemistry, University of Alberta, 11227 Saskatchewan Drive, Edmonton, Alberta, T6G 2G2, Canada

Tsz Him Chow − *Department of Physics, The Chinese University of Hong Kong, 999077 Shatin, Hong Kong SAR, China;* orcid.org/0000-0002-3884-1775

Jianfang Wang − *Department of Physics, The Chinese University of Hong Kong, 999077 Shatin, Hong Kong SAR, China;* orcid.org/0000-0002-2467-8751

Michele Magnozzi − *OptMatLab, Dipartimento di Fisica, Università di Genova, I-16146 Genova, Italy;* orcid.org/0000-0003-4512-8430

Complete contact information is available at: https://pubs.acs.org/10.1021/acs.jpcc.1c10747

Notes

The authors declare no competing financial interest.

■ ACKNOWLEDGMENTS

This work was supported by Swiss NSF via the NCCR: MUST and the European Research Council Advanced grant nos. H2020 ERCEA and 695197 DYNAMOX. L.W. acknowledges support from the China Scholarship Council (CSC). We thank Dr. Edoardo Baldini for pointing out ref 66 to us, which prompted this work.

■ REFERENCES

(1) O'Regan, B.; Grätzel, M. A Low-Cost, High-Efficiency Solar Cell Based on Dye-Sensitized Colloidal TiO2 Films. *Nature* **1991**, *353*, 737.

(2) Linic, S.; Chavez, S.; Elias, R. Flow and Extraction of Energy and Charge Carriers in Hybrid Plasmonic Nanostructures. *Nat. Mater.* **2021**, *20*, 916.

(3) Yin, P.; Tan, Y.; Fang, H.; Hegde, M.; Radovanovic, P. V. Plasmon-Induced Carrier Polarization in Semiconductor Nanocrystals. *Nat. Nanotechnol.* **2018**, *13*, 463−467.

(4) Beydoun, D.; Amal, R.; Low, G.; McEvoy, S. Role of Nanoparticles in Photocatalysis. *J. Nanopart. Res.* **1999**, *1*, 439−458.

(5) Brongersma, M. L.; Halas, N. J.; Nordlander, P. Plasmon-Induced Hot Carrier Science and Technology. *Nat. Nanotechnol.* **2015**, *10*, 25.

(6) Shi, X.; Ueno, K.; Oshikiri, T.; Sun, Q.; Sasaki, K.; Misawa, H. Enhanced Water Splitting under Modal Strong Coupling Conditions. *Nat. Nanotechnol.* **2018**, *13*, 953−958.

(7) Wood, C. S.; Stevens, M. M. Improving the Image of Nanoparticles. *Nature* **2016**, *539*, 505−506.

(8) Baffou, G.; Cichos, F.; Quidant, R. Applications and Challenges of Thermoplasmonics. *Nat. Mater.* **2020**, *19*, 946−958.

(9) Harmsen, S.; Huang, R.; Wall, M. A.; Karabeber, H.; Samii, J. M.; Spaliviero, M.; White, J. R.; Monette, S.; O'Connor, R.; et al. Surface-Enhanced Resonance Raman Scattering Nanostars for High-Precision Cancer Imaging. *Sci. Transl. Med.* **2015**, *7*, 271ra7.

(10) O'Neal, D. P.; Hirsch, L. R.; Halas, N. J.; Payne, J. D.; West, J. L. Photo-Thermal Tumor Ablation in Mice Using near Infrared-Absorbing Nanoparticles. *Cancer Lett.* **2004**, *209*, 171−176.

(11) Rastinehad, A. R.; Anastos, H.; Wajswol, E.; Winoker, J. S.; Sfakianos, J. P.; Doppalapudi, S. K.; Carrick, M. R.; Knauer, C. J.; Taouli, B.; Lewis, S. C.; et al. Gold Nanoshell-Localized Photothermal Ablation of Prostate Tumors in a Clinical Pilot Device Study. *Proc. Natl. Acad. Sci. U.S.A.* **2019**, *116*, 18590−18596.

(12) Fang, Z.; Zhen, Y.-R.; Neumann, O.; Polman, A.; García de Abajo, F. J.; Nordlander, P.; Halas, N. J. Evolution of Light-Induced Vapor Generation at a Liquid-Immersed Metallic Nanoparticle. *Nano Lett.* **2013**, *13*, 1736−1742.

(13) Choudhuri, B.; Mondal, A.; Dhar, J. C.; Singh, N. K.; Goswami, T.; Chattopadhyay, K. K. Enhanced Photocurrent from Generated Photothermal Heat in Indium Nanoparticles Embedded TiO2 Film. *Appl. Phys. Lett.* **2013**, *102*, 233108.

(14) Mukherjee, S.; Libisch, F.; Large, N.; Neumann, O.; Brown, L. V.; Cheng, J.; Lassiter, J. B.; Carter, E. A.; Nordlander, P.; Halas, N. J. Hot Electrons Do the Impossible: Plasmon-Induced Dissociation of H2 on Au. *Nano Lett.* **2013**, *13*, 240−247.

(15) Govorov, A. O.; Richardson, H. H. Generating Heat with Metal Nanoparticles. *Nano Today* **2007**, *2*, 30−38.

(16) Richardson, H. H.; Carlson, M. T.; Tandler, P. J.; Hernandez, P.; Govorov, A. O. Experimental and Theoretical Studies of Light-

to-Heat Conversion and Collective Heating Effects in Metal Nanoparticle Solutions. *Nano Lett.* **2009**, *9*, 1139−1146.
(17) Lukianova-Hleb, E.; Hu, Y.; Latterini, L.; Tarpani, L.; Lee, S.; Drezek, R. A.; Hafner, J. H.; Lapotko, D. O. Plasmonic Nanobubbles as Transient Vapor Nanobubbles Generated around Plasmonic Nanoparticles. *ACS Nano* **2010**, *4*, 2109−2123.
(18) Carlson, M. T.; Green, A. J.; Richardson, H. H. Superheating Water by CW Excitation of Gold Nanodots. *Nano Lett.* **2012**, *12*, 1534−1537.
(19) Neumann, O.; Urban, A. S.; Day, J.; Lal, S.; Nordlander, P.; Halas, N. J. Solar Vapor Generation Enabled by Nanoparticles. *ACS Nano* **2013**, *7*, 42−49.
(20) Yeshchenko, O. A.; Kutsevol, N. V.; Naumenko, A. P. Light-Induced Heating of Gold Nanoparticles in Colloidal Solution: Dependence on Detuning from Surface Plasmon Resonance. *Plasmonics* **2016**, *11*, 345−350.
(21) Ferrera, M.; Della Valle, G.; Sygletou, M.; Magnozzi, M.; Catone, D.; O'Keeffe, P.; Paladini, A.; Toschi, F.; Mattera, L.; et al. Thermometric Calibration of the Ultrafast Relaxation Dynamics in Plasmonic Au Nanoparticles. *ACS Photonics* **2020**, *7*, 959−966.
(22) Hache, F.; Ricard, D.; Flytzanis, C.; Kreibig, U. The Optical Kerr Effect in Small Metal Particles and Metal Colloids: The Case of Gold. *Appl. Phys. A* **1988**, *47*, 347−357.
(23) Perner, M.; Bost, P.; Lemmer, U.; von Plessen, G.; Feldmann, J.; Becker, U.; Mennig, M.; Schmitt, M.; Schmidt, H. Optically Induced Damping of the Surface Plasmon Resonance in Gold Colloids. *Phys. Rev. Lett.* **1997**, *78*, 2192−2195.
(24) Inouye, H.; Tanaka, K.; Tanahashi, I.; Hirao, K. Ultrafast Dynamics of Nonequilibrium Electrons in a Gold Nanoparticle System. *Phys. Rev. B: Condens. Matter Mater. Phys.* **1998**, *57*, 11334.
(25) Sasai, J.; Hirao, K. Relaxation Behavior of Nonlinear Optical Response in Borate Glasses Containing Gold Nanoparticles. *J. Appl. Phys.* **2001**, *89*, 4548−4553.
(26) Mohamed, M. B.; Ahmadi, T. S.; Link, S.; Braun, M.; El-Sayed, M. A. Hot Electron and Phonon Dynamics of Gold Nanoparticles Embedded in a Gel Matrix. *Chem. Phys. Lett.* **2001**, *343*, 55−63.
(27) Link, S.; Furube, A.; Mohamed, M. B.; Asahi, T.; Masuhara, H.; El-Sayed, M. A. Hot Electron Relaxation Dynamics of Gold Nanoparticles Embedded in MgSO4 Powder Compared To Solution:The Effect of the Surrounding Medium. *J. Phys. Chem. B* **2002**, *106*, 945−955.
(28) Katayama, T.; Setoura, K.; Werner, D.; Miyasaka, H.; Hashimoto, S. Picosecond-to-Nanosecond Dynamics of Plasmonic Nanobubbles from Pump−Probe Spectral Measurements of Aqueous Colloidal Gold Nanoparticles. *Langmuir* **2014**, *30*, 9504−9513.
(29) Stoll, T.; Maioli, P.; Crut, A.; Rodal-Cedeira, S.; Pastoriza-Santos, I.; Vallée, F.; Del Fatti, N. Time-Resolved Investigations of the Cooling Dynamics of Metal Nanoparticles: Impact of Environment. *J. Phys. Chem. C* **2015**, *119*, 12757−12764.
(30) Minutella, E.; Schulz, F.; Lange, H. Excitation-Dependence of Plasmon-Induced Hot Electrons in Gold Nanoparticles. *J. Phys. Chem. Lett.* **2017**, *8*, 4925−4929.
(31) Zhang, X.; Huang, C.; Wang, M.; Huang, P.; He, X.; Wei, Z. Transient Localized Surface Plasmon Induced by Femtosecond Interband Excitation in Gold Nanoparticles. *Sci. Rep.* **2018**, *8*, 10499.
(32) Aiboushev, A.; Gostev, F.; Shelaev, I.; Kostrov, A.; Kanaev, A.; Museur, L.; Traore, M.; Sarkisov, O.; Nadtochenko, V. Spectral Properties of the Surface Plasmon Resonance and Electron Injection from Gold Nanoparticles to TiO2 Mesoporous Film: Femtosecond Study. *Photochem. Photobiol. Sci.* **2013**, *12*, 631−637.
(33) Radzig, M.; Koksharova, O.; Khmel, I.; Ivanov, V.; Yorov, K.; Kiwi, J.; Rtimi, S.; Tastekova, E.; Aybush, A.; et al. Femtosecond Spectroscopy of Au Hot-Electron Injection into TiO2: Evidence for Au/TiO2 Plasmon Photocatalysis by Bactericidal Au Ions and Related Phenomena. *Nanomaterials* **2019**, *9*, 217.
(34) Hodak, J. H.; Henglein, A.; Hartland, G. V. Photophysics of Nanometer Sized Metal Particles:Electron−Phonon Coupling and Coherent Excitation of Breathing Vibrational Modes. *J. Phys. Chem. B* **2000**, *104*, 9954−9965.
(35) Ahmadi, T. S.; Logunov, S. L.; El-Sayed, M. A. Picosecond Dynamics of Colloidal Gold Nanoparticles. *J. Phys. Chem.* **1996**, *100*, 8053−8056.
(36) Logunov, S. L.; Ahmadi, T. S.; El-Sayed, M. A.; Khoury, J. T.; Whetten, R. L. Electron Dynamics of Passivated Gold Nanocrystals Probed by Subpicosecond Transient Absorption Spectroscopy. *J. Phys. Chem. B* **1997**, *101*, 3713−3719.
(37) Groeneveld, R. H. M.; Sprik, R.; Lagendijk, A. Femtosecond Spectroscopy of Electron-Electron and Electron-Phonon Energy Relaxation in Ag and Au. *Phys. Rev. B: Condens. Matter Mater. Phys.* **1995**, *51*, 11433.
(38) Hodak, J.; Martini, I.; Hartland, G. V. Ultrafast Study of Electron−Phonon Coupling in Colloidal Gold Particles. *Chem. Phys. Lett.* **1998**, *284*, 135−141.
(39) Wang, L.; Rossi, T.; Oppermann, M.; Bauer, B.; Mewes, L.; Zare, D.; Chow, T. H.; Wang, J.; Chergui, M. Slow Charge Carrier Relaxation in Gold Nanoparticles. *J. Phys. Chem. C* **2020**, *124*, 24322−24330.
(40) Hu, M.; Wang, X.; Hartland, G. V.; Salgueiriño-Maceira, V.; Liz-Marzán, L. M. Heat Dissipation in Gold−Silica Core-Shell Nanoparticles. *Chem. Phys. Lett.* **2003**, *372*, 767−772.
(41) Hu, M.; Hartland, G. V. Heat Dissipation for Au Particles in Aqueous Solution: Relaxation Time versus Size. *J. Phys. Chem. B* **2002**, *106*, 7029−7033.
(42) Hartland, G. V.; Besteiro, L. V.; Johns, P.; Govorov, A. O. What's so Hot about Electrons in Metal Nanoparticles? *ACS Energy Lett.* **2017**, *2*, 1641−1653.
(43) O'Keeffe, P.; Catone, D.; Di Mario, L.; Toschi, F.; Magnozzi, M.; Bisio, F.; Alabastri, A.; Proietti Zaccaria, R.; et al. Disentangling the Temporal Dynamics of Nonthermal Electrons in Photoexcited Gold Nanostructures. *Laser Photon. Rev.* **2021**, *15*, 2100017.
(44) Doremus, R. H. Optical Properties of Small Gold Particles. *J. Chem. Phys.* **1964**, *40*, 2389−2396.
(45) Kawabata, A.; Kubo, R. Electronic Properties of Fine Metallic Particles. II. Plasma Resonance Absorption. *J. Phys. Soc. Jpn.* **1966**, *21*, 1765−1772.
(46) Kruglyak, V. V.; Hicken, R. J.; Matousek, P.; Towrie, M. Spectroscopic Study of Optically Induced Ultrafast Electron Dynamics in Gold. *Phys. Rev. B: Condens. Matter Mater. Phys.* **2007**, *75*, 035410.
(47) Schoenlein, R. W.; Lin, W. Z.; Fujimoto, J. G.; Eesley, G. L. Femtosecond Studies of Nonequilibrium Electronic Processes in Metals. *Phys. Rev. Lett.* **1987**, *58*, 1680.
(48) Sun, C.-K.; Vallée, F.; Acioli, L. H.; Ippen, E. P.; Fujimoto, J. G. Femtosecond-Tunable Measurement of Electron Thermalization in Gold. *Phys. Rev. B: Condens. Matter Mater. Phys.* **1994**, *50*, 15337−15348.
(49) Stoll, T.; Maioli, P.; Crut, A.; Rodal-Cedeira, S.; Pastoriza-Santos, I.; Vallée, F.; Del Fatti, N. Time-Resolved Investigations of the Cooling Dynamics of Metal Nanoparticles: Impact of Environment. *J. Phys. Chem. C* **2015**, *119*, 12757−12764.
(50) Yeshchenko, O. A.; Bondarchuk, I. S.; Gurin, V. S.; Dmitruk, I. M.; Kotko, A. V. Temperature Dependence of the Surface Plasmon Resonance in Gold Nanoparticles. *Surf. Sci.* **2013**, *608*, 275−281.
(51) Bouillard, J.-S. G.; Dickson, W.; O'Connor, D. P.; Wurtz, G. A.; Zayats, A. V. Low-Temperature Plasmonics of Metallic Nanostructures. *Nano Lett.* **2012**, *12*, 1561−1565.
(52) Link, S.; El-Sayed, M. A. Size and Temperature Dependence of the Plasmon Absorption of Colloidal Gold Nanoparticles. *J. Phys. Chem. B* **1999**, *103*, 4212−4217.
(53) Magnozzi, M.; Ferrera, M.; Mattera, L.; Canepa, M.; Bisio, F. Plasmonics of Au Nanoparticles in a Hot Thermodynamic Bath. *Nanoscale* **2019**, *11*, 1140−1146.
(54) Ruan, Q.; Shao, L.; Shu, Y.; Wang, J.; Wu, H. Growth of Monodisperse Gold Nanospheres with Diameters from 20 Nm to

https://doi.org/10.1021/acs.jpcc.1c10747
J. Phys. Chem. C 2022, 126, 3591−3599

220 Nm and Their Core/Satellite Nanostructures. *Adv. Opt. Mater.* **2014**, *2*, 65−73.
(55) Mooney, J.; Kambhampati, P. Get the Basics Right: Jacobian Conversion of Wavelength and Energy Scales for Quantitative Analysis of Emission Spectra. *J. Phys. Chem. Lett.* **2013**, *4*, 3316−3318.
(56) Juvé, V.; Scardamaglia, M.; Maioli, P.; Crut, A.; Merabia, S.; Joly, L.; Del Fatti, N.; Vallée, F. Cooling Dynamics and Thermal Interface Resistance of Glass-Embedded Metal Nanoparticles. *Phys. Rev. B: Condens. Matter Mater. Phys.* **2009**, *80*, 195406.
(57) Voisin, C.; Del Fatti, N.; Christofilos, D.; Vallée, F. Ultrafast Electron Dynamics and Optical Nonlinearities in Metal Nanoparticles. *J. Phys. Chem. B* **2001**, *105*, 2264−2280.
(58) Wray, J. H.; Neu, J. T. Refractive Index of Several Glasses as a Function of Wavelength and Temperature. *J. Opt. Soc. Am.* **1969**, *59*, 774.
(59) Schiebener, P.; Straub, J.; Levelt Sengers, J. M. H.; Gallagher, J. S. Refractive Index of Water and Steam as Function of Wavelength, Temperature and Density. *J. Phys. Chem. Ref. Data* **1990**, *19*, 677−717.
(60) Hale, G. M.; Querry, M. R. Optical Constants of Water in the 200-Nm to 200-Mm Wavelength Region. *Appl. Opt.* **1973**, *12*, 555−563.
(61) Magnozzi, M.; Terreni, S.; Anghinolfi, L.; Uttiya, S.; Carnasciali, M. M.; Gemme, G.; Neri, M.; Principe, M.; Pinto, I.; et al. Optical Properties of Amorphous SiO2-TiO2 Multi-Nanolayered Coatings for 1064-Nm Mirror Technology. *Opt. Mater.* **2018**, *75*, 94−101.
(62) Magnozzi, M.; Ferrera, M.; Mattera, L.; Canepa, M.; Bisio, F. Plasmonics of Au Nanoparticles in a Hot Thermodynamic Bath. *Nanoscale* **2019**, *11*, 1140−1146.
(63) Magnozzi, M.; Proietti Zaccaria, R.; Catone, D.; O'Keeffe, P.; Paladini, A.; Toschi, F.; Alabastri, A.; Canepa, M.; Bisio, F. Interband Transitions Are More Efficient Than Plasmonic Excitation in the Ultrafast Melting of Electromagnetically Coupled Au Nanoparticles. *J. Phys. Chem. C* **2019**, *123*, 16943−16950.
(64) Logunov, S. L.; Ahmadi, T. S.; El-Sayed, M. A.; Khoury, J. T.; Whetten, R. L. Electron Dynamics of Passivated Gold Nanocrystals Probed by Subpicosecond Transient Absorption Spectroscopy. *J. Phys. Chem. B* **1997**, *101*, 3713−3719.
(65) Hartland, G. V. Measurements of the Material Properties of Metal Nanoparticles by Time-Resolved Spectroscopy. *Phys. Chem. Chem. Phys.* **2004**, *6*, 5263−5274.
(66) Kruglyak, V. V.; Hicken, R. J.; Matousek, P.; Towrie, M. Spectroscopic Study of Optically Induced Ultrafast Electron Dynamics in Gold. *Phys. Rev. B: Condens. Matter Mater. Phys.* **2007**, *75*, 035410.

https://doi.org/10.1021/acs.jpcc.1c10747
J. Phys. Chem. C 2022, 126, 3591−3599